Ferrofluidity in a Two-Component Dipolar Bose-Einstein Condensate

Hiroki Saito,[1] Yuki Kawaguchi,[2] and Masahito Ueda[2,3]

[1]*Department of Applied Physics and Chemistry, University of Electro-Communications, Tokyo 182-8585, Japan*
[2]*Department of Physics, University of Tokyo, Tokyo 113-0033, Japan*
[3]*ERATO Macroscopic Quantum Project, JST, Tokyo 113-8656, Japan*

(Received 1 December 2008; published 8 June 2009)

It is shown that the interface in a two-component Bose-Einstein condensate (BEC) with a dipole-dipole interaction spontaneously develops patterns similar to those formed in a ferrofluid. Hexagonal, labyrinthine, solitonlike structures, and hysteretic behavior are numerically demonstrated. Superflow is found to circulate around the hexagonal pattern at rest, offering evidence of supersolidity. The system sustains persistent current with a vortex line pinned by the hexagonal pattern. These phenomena may be realized using a ^{52}Cr BEC.

DOI: 10.1103/PhysRevLett.102.230403 PACS numbers: 03.75.Mn, 03.75.Hh, 47.65.Cb

When a magnetic liquid (a colloidal suspension of magnetic fine particles) is subjected to a magnetic field perpendicular to the surface, the liquid is magnetized and the surface undergoes a spontaneous deformation into characteristic patterns such as horns growing from the liquid. This surface instability is known as the normal field or Rosensweig instability [1] and is a subject of active research [2–8]. The system also exhibits a variety of phenomena, such as hysteretic behavior [4], a transition between hexagonal and square patterns [5], and stabilization of a solitonlike structure [8]. Because of the visual appeal of the pattern formation, the dynamics of the magnetic-liquid surfaces are displayed even in art [9].

In this Letter, we show that a Bose-Einstein condensate (BEC) of an atomic gas with a strong dipole-dipole interaction (DDI) [10] exhibits instabilities and pattern formation similar to those in magnetic liquids. We find that there are many similarities between the present system and a magnetic liquid, such as hexagonal, solitonlike, and labyrinthine [11] pattern formation and hysteretic behavior. Moreover, novel phenomena unique to the present superfluid system are found. The hexagonal pattern remains stationary even in the presence of superflow, offering new evidence of supersolidity [12]. We also show that the hexagonal pattern pins a vortex line, thereby sustaining persistent flow.

The system considered here is schematically illustrated in Fig. 1. A two-component BEC is used, in which the atoms in component 1 have a magnetic dipole moment and the atoms in component 2 are nonmagnetic. A magnetic field is applied to fix the direction of the fully polarized magnetic dipoles (say, in the z direction). A magnetic-field gradient in the z direction pulls the atoms in component 1 in the $-z$ direction, so that the two components separate as illustrated in Fig. 1. In analogy with a magnetic-liquid system, the interface between the two components corresponds to the magnetic-liquid surface, the field gradient plays the role of gravity, and the quantum pressure and contact interatomic interactions create an interface energy, corresponding to the surface tension of a magnetic liquid. The Rosensweig instability in magnetic liquids occurs when it lowers the sum of magnetic, surface, and gravitational energies.

A two-component BEC is used because texture formation [13] is energetically more favorable than density-pattern formation. For the density pattern to be formed in a single-component BEC [14,15], the DDI must overcome the contact interaction, which however leads to a dipolar collapse [16]. Quasi-two-dimensional (2D) systems have been considered as a way of stabilizing density patterns (2D solitons) without a dipolar collapse [17,18]. Use of a multicomponent dipolar BEC [19] is another possible way of creating pattern formation without suffering a dipolar collapse.

We consider a two-component BEC described by the macroscopic wave functions ψ_1 and ψ_2 in the zero-temperature mean-field approximation. The wave functions obey the nonlocal Gross-Pitaevskii (GP) equations

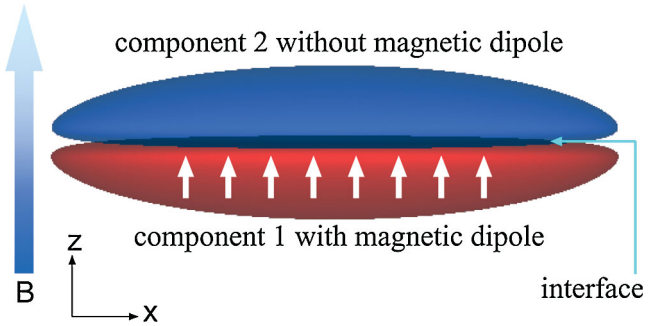

FIG. 1 (color). Schematic illustration of the system. A two-component BEC is confined in a trapping potential, in which component 1 has a magnetic dipole moment and component 2 does not. The magnetic dipole is polarized in the z direction by an external magnetic field. The two components are separated due to the field gradient $B'(z) < 0$.

given by

$$i\hbar\frac{\partial\psi_1}{\partial t} = \left(-\frac{\hbar^2\nabla^2}{2M_1} + V_1 - \mu B'z + g_{11}|\psi_1|^2 + g_{12}|\psi_2|^2 + \int U(\boldsymbol{r}-\boldsymbol{r}')|\psi_1(\boldsymbol{r}')|^2 d\boldsymbol{r}'\right)\psi_1, \quad (1a)$$

$$i\hbar\frac{\partial\psi_2}{\partial t} = \left(-\frac{\hbar^2\nabla^2}{2M_2} + V_2 + g_{22}|\psi_2|^2 + g_{12}|\psi_1|^2\right)\psi_2, \quad (1b)$$

where M_n and V_n are the atomic mass and trap potential for component $n = 1$ or 2. The coupling constants are given by $g_{nn'} = 2\pi\hbar^2 a_{nn'}/M_{nn'}$ with $a_{nn'}$ and $M_{nn'}$ being the s-wave scattering length and the reduced mass between components n and n'. The DDI has the form $U(\boldsymbol{r}) = \mu_0\mu^2(1 - 3z^2/r^2)/(4\pi r^3)$, where μ_0 is the magnetic permeability of vacuum and μ is the magnetic dipole moment of the atom in component 1. For simplicity, we assume that the two components have the same mass M and the same number of atoms $N/2$ and that they experience the same axisymmetric harmonic potential given by $V_n = M/2[\omega_\perp^2(x^2 + y^2) + \omega_z^2 z^2]$, where $\omega_\perp$ and ω_z are the radial and axial trap frequencies. Gravity only shifts the origin and can be neglected. The magnetic field depends only on z, and $dB/dz \equiv B'$ is uniform. We assume $\mu = 6\mu_B$ and $a_{11} = a_{22} = a_{12} = 100a_B$ with μ_B and a_B being the Bohr magneton and the Bohr radius, respectively, and take M to be the mass of a ^{52}Cr atom.

We first investigate stationary states of the system, obtained by replacing i with -1 on the left-hand sides of Eqs. (1a) and (1b). The numerical propagation is performed using the Crank-Nicolson scheme and the dipolar part is calculated using a fast Fourier transform. The initial state of the imaginary-time propagation is a flat-interface state Ψ_n for a sufficiently large $|B'|$ with small initial noise $\psi_n = \Psi_n + r_n$, where r_n represents a small complex number randomly chosen for each mesh.

Figure 2(a) shows an isodensity surface of component 1 for $B' = -1$ G/cm. The hexagonal density bumps on the interface between the two components resemble the Rosensweig pattern on a magnetic-liquid surface. Since the density is high and hence the DDI is large at the center of the trap, the peaks around the center are higher than those on the periphery. Figure 2(b) shows the column-density profiles integrated along the z axis. Components 1 and 2 exhibit a phase separation in the x-y plane [left and middle panels of Fig. 2(b)], since the DDI is attractive in component 1, resulting in an effective immiscible condition.

When the field gradient is increased or the number of atoms is decreased, the number and height of the peaks decrease [Figs. 2(c) and 2(e)] and eventually the interface becomes flat [Fig. 2(d)]. There is hysteresis with respect to a change in the field gradient. When $|B'|$ is increased from 1 G/cm, the hexagonal pattern reduces to a single peak [Fig. 2(c)], which then disappears at $B' \lesssim -1.66$ G/cm.

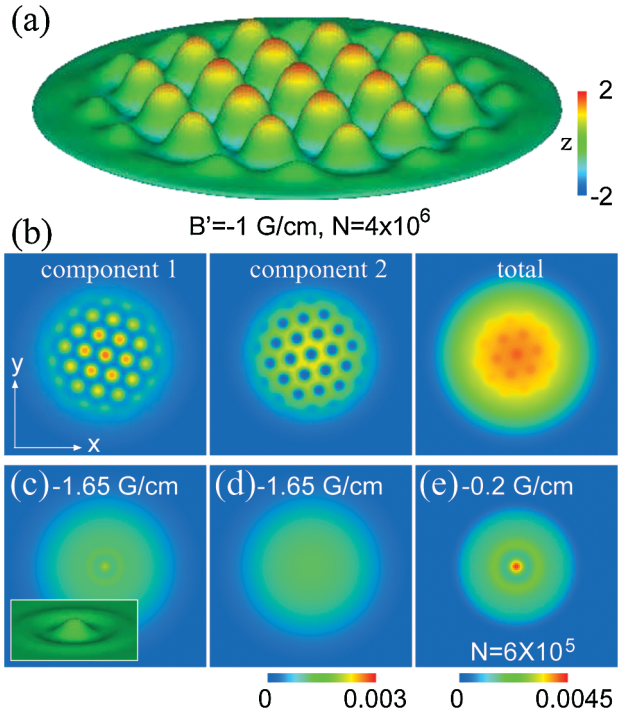

FIG. 2 (color). Stationary states of the two-component dipolar BEC for $a_{11} = a_{22} = a_{12} = 100a_B$ and $\mu = 6\mu_B$ in an axisymmetric potential with $(\omega_\perp, \omega_z) = 2\pi \times (100, 800)$ Hz. (a) Isodensity surface of component 1 and (b) column densities $\int|\psi_1|^2 dz$, $\int|\psi_2|^2 dz$, and $\int(|\psi_1|^2 + |\psi_2|^2)dz$ normalized by $NM\omega_\perp/\hbar$ for the field gradient $B' = -1$ G/cm. The color in (a) represents the z coordinate in units of $(\hbar/M\omega_\perp)^{1/2}$. (c)–(d) Column densities of component 1 for $B' = -1.65$ G/cm (bistable). The inset in (c) shows isodensity surface near the central peak. The total number of atoms is $N = 4 \times 10^6$ for (a)–(d) with an equal population in each component. (e) Column density of component 1 for $N = 6 \times 10^5$ and $B' = -0.2$ G/cm. The color gauge is 0-0.003 for (b)–(d) and 0-0.0045 for (e). The field of view for (b)–(e) is 50×50 μm.

On the other hand, when $|B'|$ is decreased from a large value, the interface remains flat [Fig. 2(d)] for $B' \lesssim -1.64$ G/cm. Therefore, there is a bistable region around $|B'| \simeq 1.65$ G/cm, in which the single-peaked state and the flat-interface state are bistable. In the bistability region, the energies of the two states are almost degenerate. The hysteresis can be demonstrated by real-time propagation of the GP equation with an adiabatic change in the field gradient. Such hysteretic behavior has been predicted [3,7] and observed [4,8] for magnetic liquids. The single-peaked structure in the bistable region, as shown in Fig. 2(c), is reminiscent of the "ferrosoliton" [8] in a magnetic liquid, which is a stable solitonlike peak. Around the peak, the interface oscillates in a concentric manner [inset in Fig. 2(c)], as in the ferrosoliton [8].

There are various metastable patterns for smaller values of the field gradient, as shown in Fig. 3 for $B' = -0.3$ G/cm. To trigger these various pattern formations, we use various initial seeds. For example, Fig. 3(a) is obtained by applying an additional magnetic field

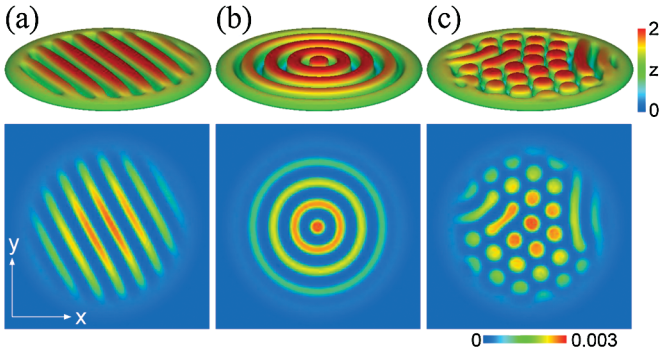

FIG. 3 (color). Isodensity surface (upper panels) and integrated column density (lower panels) of component 1 for various stationary states. The difference among (a)–(c) arises only from initial seeds in the imaginary-time propagation. The field gradient is $B' = -0.3$ G/cm. The other parameters are the same as those in Fig. 2(a).

$\propto \sin(k_x x + k_y y)$ for $t < 1$ ms in the imaginary-time propagation, where $k_x a_\perp = \sqrt{3}$ and $k_y a_\perp = 1$ with $a_\perp = (\hbar/M\omega_\perp)^{1/2}$. We find that the imaginary-time propagation relaxes the system to the stripe pattern as shown in Fig. 3(a). This pattern is robust against small perturbations. The initial temporary magnetic field for Fig. 3(b) is $\propto \cos(\sqrt{x^2 + y^2}/a_\perp)$. The concentric pattern in Fig. 3(b) is stable against axisymmetry breaking perturbations. Figure 3(c) is obtained without an additional magnetic field, with only small random seeds added to the initial state. These results imply that there are many metastable states with various patterns. In Fig. 3(c), the peaks partly merge with each other. The merging of the peaks tends to occur for a large DDI and a small field gradient. For $B' = -1$ G/cm, the stripe and concentric patterns in Figs. 3(a) and 3(b) are unstable against peak formation.

A striking difference between the present system and magnetic liquids is that the present system is a superfluid, while a conventional magnetic liquid is a normal fluid. Figure 4 shows a stationary state with component 1 having a vortex line at $x = y = 0$. The Rosensweig pattern emerges even in the presence of superflow. We note that the pattern in Fig. 4(a) is stationary and does not rotate in the laboratory frame despite the fact that the superflow circulates as shown in Fig. 4(c). This situation has a close analogy to supersolidity [12], where crystalline order and superflow coexist. We also note that the vortex line in Fig. 4 is pinned at $x = y = 0$ by the surrounding peaks. The system therefore sustains persistent flow without any external pinning potential.

If component 2 has a magnetic dipole moment opposite to that of component 1, a quite different pattern is formed. Figure 5 shows a stationary state of the system, in which components 1 and 2 have magnetic moments $6\mu_B$ and $-6\mu_B$, respectively. The intricate pattern shown in Figs. 5(a) and 5(b) is reminiscent of the labyrinthine pattern in an immiscible magnetic and nonmagnetic liquids confined in a thin layer [11]. The pattern formation occurs even for $N = 10^5$ as shown in Fig. 5(c), which can be realized in current experiments. Since magnetic liquids are paramagnetic (not diamagnetic), a mixture of two fluids with opposite magnetizations is impossible. For a BEC, by contrast, a magnetic moment of each atom is conserved if spin exchange is suppressed, and a mixture of opposite magnetic moments, such as $m_J = \pm 3$ of ^{52}Cr, is maintained once it is created by, e.g., the rf technique.

Next we study the dynamics of the pattern formation in a nondissipative system by solving the real-time propagation of Eq. (1). Figure 6 shows the time evolution of the system, where the initial state is a flat-interface state for $B' = -1.7$ G/cm and other conditions are the same as those in Fig. 2. We let the system evolve in time with $B' = -1$ G/cm, for which the stable state has hexagonal peaks, as shown in Fig. 2(a). The density fluctuations grow to form many peaks, as in Figs. 6(b) and 6(c), due to the Rosensweig instability. We note that the characteristic wavelength in the pattern at an early stage [Fig. 6(b)] is smaller than that at a later stage [Fig. 6(c)]. This difference indicates that the most unstable wavelength in the linear regime does not correspond to the final stable pattern determined by the nonlinear interaction. A similar situation also occurs in magnetic liquids [6]. If the phenomenological dissipation is taken into account by replacing i with, e.g., $i - 0.03$ [20] in Eq. (1), the hexagonal pattern is formed at ~50 ms.

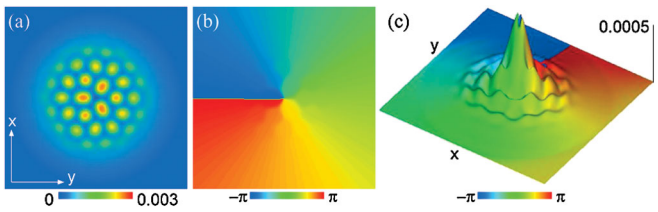

FIG. 4 (color). (a) Column density of component 1 and (b) $\arg\psi_1(z = 0)$ for a stationary state, in which component 1 has a vortex line at $x = y = 0$ and component 2 has no vortex. (c) Magnitude $(J_x^2 + J_y^2)^{1/2}$ (height) and direction $\arg(J_x + iJ_y)$ (color) of the atomic flow $\boldsymbol{J} = a_\perp^3 \int \mathrm{Im}\psi_1^* \nabla \psi_1 dz$. The parameters are the same as those in Fig. 2(a).

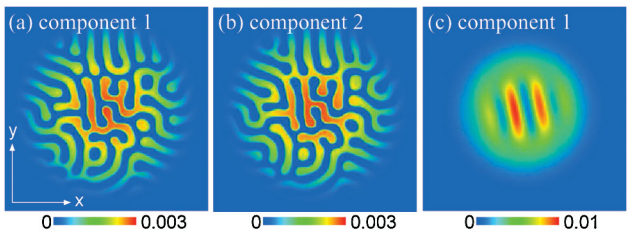

FIG. 5 (color). Column density for stationary states, in which components 1 and 2 have magnetic dipole moments $6\mu_B$ and $-6\mu_B$, respectively. The field gradient is $B' = 0$. (a) and (b) $N = 4 \times 10^6$. (c) $N = 10^5$. The field of view is 50×50 μm for (a) and (b), and 30×30 μm for (c).

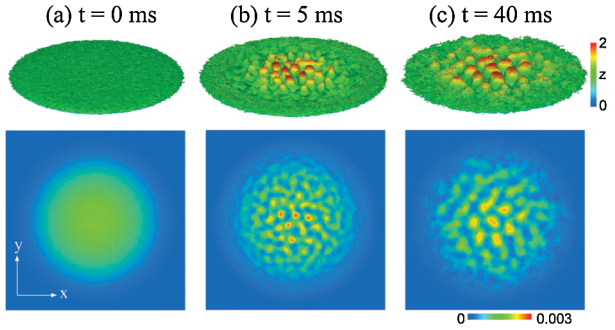

FIG. 6 (color). Time evolution of the isodensity surface (upper figures) and that of the column density (lower panels) of component 1. The initial state is the flat-interface state for $B' = -1.7$ G/cm and the field gradient changes to $B' = -1$ G/cm at $t = 0$. The field of view is 50×50 μm. The parameters are the same as those in Fig. 2(a).

A candidate for components 1 and 2 is the $^7S_3$ $m_J = -3$ and 0 states of a ^{52}Cr atom. Though the $m_J \neq -3$ states are unstable against dipolar collisions, the lifetime is long enough ($\sim$ s) [10] to observe the pattern-formation dynamics, unless the external magnetic field is too small ($\lesssim$1 mG). The spin-exchange dynamics, such as $m_J = 0$, $0 \rightarrow -3$, 3 [21], can be suppressed using, e.g., the laser-induced quadratic Zeeman effect [22,23]. The scattering lengths measured in Ref. [24] give $a_{22} \simeq 60.7a_B + a_0/7$ and $a_{12} \simeq 67.8a_B$, with a_0 being the scattering length for the colliding channel with total spin 0, which is unknown. The scattering length a_{11} can be controlled using the magnetic Feshbach resonance [25], where the resonance width 1.7 G [24] is much broader than the inhomogeneity of the magnetic field $\sim$1 G/cm $\times$ 10 μm. We can therefore realize $a_{11} \sim a_{22} \sim a_{12} \sim 60a_B$ by changing a_{11}, if $|a_0|$ is not very large. We have confirmed that the Rosensweig pattern emerges for these scattering lengths. Another possibility for component 2 is an alkali atom, for which, however, a_{12} has not been measured yet. The situation in Fig. 5 is realized with the $m_J = 3$ state of ^{52}Cr for component 2, where the spin-exchange dynamics can be suppressed by a negative quadratic Zeeman energy [22]. In this case, $a_{11} = a_{22} \simeq 100a_B$ and $a_{12} \simeq 2.85a_B + 2a_0/7$ is assumed to be tuned to $\sim 100a_B$.

If the dipole moment of component 1 is decreased to $\mu_B/2$, which corresponds to spin-1 alkali atoms, N must be $\sim 10^8$ for the same trap frequencies and the same scattering lengths as those in Fig. 2. We can reduce N to $\simeq 1.0 \times 10^5$, if polar molecules with an electric dipole moment of 0.1 Debye are used. For the same trap frequencies and magnetic dipole moment as those in Fig. 2, the scattering lengths can be $(a_{11}, a_{22}, a_{12}) \simeq (100, 85 - 108, 100)a_B$ and $(100, 100, \gtrsim 97)a_B$. There is a scaling property characterized by dimensionless parameters, $Na_{ij}/a_\perp$, $\mu_0\mu^2 N/(\hbar\omega_\perp a_\perp^3)$, $\mu B' a_\perp/(\hbar\omega_\perp)$, and $\omega_z/\omega_\perp$, and similar phenomena should be observed for the same set of these parameters. For example, the situation in Fig. 2(e) can also be realized for $N = 10^5$ and $(\omega_\perp, \omega_z) = 2\pi \times (3.6, 28.8)$ kHz.

In conclusion, we have studied pattern formation on the interface in a two-component BEC with a DDI. We found various interfacial patterns, including Rosensweig hexagonal peaks and a labyrinthine pattern. We also observed hysteretic behavior and the ferrosoliton, as in magnetic liquids. The novelty of the present system compared with magnetic liquids is that superflow can circulate around the Rosensweig pattern at rest, which provides new evidence of supersolidity. The Rosensweig peaks pins a vortex line and the system sustains persistent current. The two-component system proposed here thus exhibits a rich variety of phenomena, which may be realized using a BEC of ^{52}Cr atoms or polar molecules.

This work was supported by MEXT Japan (KAKENHI No. 17071005 and No. 20540388, and the Global COE Program "the Physical Sciences Frontier") and by the Matsuo Foundation.

[1] M. D. Cowley and R. E. Rosensweig, J. Fluid Mech. **30**, 671 (1967).
[2] R. E. Rosensweig, *Ferrohydrodynamics* (Cambridge Univ. Press, Cambridge, 1985) and references therein.
[3] A. Gailitis, J. Fluid Mech. **82**, 401 (1977).
[4] J.-C. Bacri and D. Salin, J. Phys. Lett. **45**, 559 (1984).
[5] D. Allais and J.-E. Wesfreid, Bull. Soc. Fr. Phys. Suppl. **57**, 20 (1985); B. Abou *et al.*, J. Fluid Mech. **416**, 217 (2000).
[6] A. Lange *et al.*, Phys. Rev. E **61**, 5528 (2000).
[7] R. Friedrichs and A. Engel, Phys. Rev. E **64**, 021406 (2001).
[8] R. Richter and I. V. Barashenkov, Phys. Rev. Lett. **94**, 184503 (2005).
[9] See, e.g., S. Kodama, Commun. ACM **51**, 79 (2008).
[10] A. Griesmaier *et al.*, Phys. Rev. Lett. **94**, 160401 (2005).
[11] L. T. Romankiw *et al.*, IEEE Trans. Magn. **11**, 25 (1975).
[12] A. F. Andreev and I. M. Lifshitz, Sov. Phys. JETP **29**, 1107 (1969); G. V. Chester, Phys. Rev. A **2**, 256 (1970); A. J. Leggett, Phys. Rev. Lett. **25**, 1543 (1970).
[13] J. Stenger *et al.*, Nature (London) **396**, 345 (1998).
[14] S. Ronen *et al.*, Phys. Rev. Lett. **98**, 030406 (2007).
[15] R. M. Wilson *et al.*, Phys. Rev. Lett. **100**, 245302 (2008).
[16] T. Lahaye *et al.*, Phys. Rev. Lett. **101**, 080401 (2008).
[17] P. Pedri and L. Santos, Phys. Rev. Lett. **95**, 200404 (2005).
[18] I. Tikhonenkov *et al.*, Phys. Rev. Lett. **100**, 090406 (2008).
[19] K. Góral and L. Santos, Phys. Rev. A **66**, 023613 (2002).
[20] M. Tsubota *et al.*, Phys. Rev. A **65**, 023603 (2002).
[21] L. Santos and T. Pfau, Phys. Rev. Lett. **96**, 190404 (2006).
[22] L. Santos *et al.*, Phys. Rev. A **75**, 053606 (2007).
[23] $m_J = 0$, $0 \rightarrow -3$, 3, and -3, $0 \rightarrow -2$, -1 cannot be suppressed simultaneously by the method in Ref. [22]. However, the latter process is negligible for $\sim$100 ms because of the lack of initial seeds in $m_J = -2$ and -1, and because of the phase separation between $m_J = -3$ and 0.
[24] J. Werner *et al.*, Phys. Rev. Lett. **94**, 183201 (2005).
[25] T. Lahaye *et al.*, Nature (London) **448**, 672 (2007).